THE JOURNAL OF PHYSICAL CHEMISTRY B

Article

pubs.acs.org/JPCB

Dendritic Amphiphiles Strongly Affect the Biophysical Properties of DPPC Bilayer Membranes

Riya J. Muckom,[†] Francesca Stanzione,[†] Richard D. Gandour,[‡] and Amadeu K. Sum*[,†]

[†]Chemical and Biological Engineering Department, Colorado School of Mines, 1600 Illinois Street, Golden, Colorado, United States

[‡]Department of Chemistry (0212) and Virginia Tech Center for Drug Discovery, Virginia Tech, Blacksburg, Virginia 24061, United States

Supporting Information

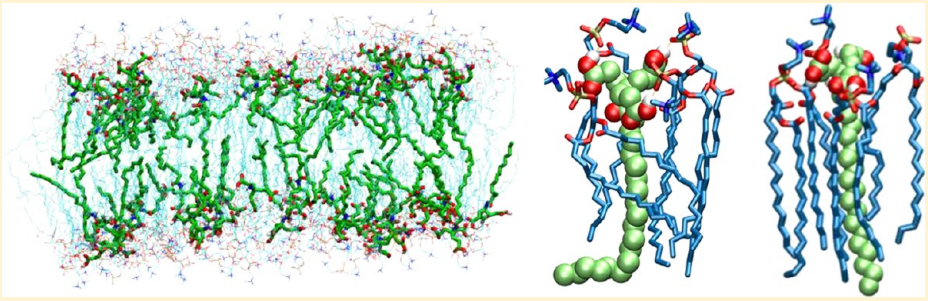

ABSTRACT: Molecular dynamics (MD) simulations were used to gain insight on the molecular interactions in a model biological membrane comprised of a bilayer with DPPC (dipalmitoylphosphotidylcholine) and antimicrobial dendritic amphiphile molecules [$RCONHC(CH_2CH_2COOH)_3$, where R is the saturated hydrocarbon tail (R = n-C_nH_{2n+1}), to be abbreviated as 3CAmn]. This study analyzes different biophysical properties of the equilibrated mixed bilayers, at 300 and 325 K, to determine how the presence of the 3CAmn, in varying concentrations and tail lengths, affects the lipid bilayer. Lipid tail order parameter data, bilayer thickness trends, and qualitative lipid tail tilt observations suggest that a molar ratio of 0.2 3CAm19/DPPC is sufficient to induce a phase transition in the bilayer from gel to liquid crystalline at 300 K. These results also imply that the phase transition temperature of the mixed bilayer decreases upon incorporation of higher concentrations of 3CAm19. Hydrogen bonding takes place between the 3CAmn and DPPC at specific sites, as evidenced by the radial distribution function. Increased hydrogen bonding and the smaller headgroup size of the 3CAmn molecule result in a decrease in the total lateral area with higher concentrations of 3CAm19. Diffusion constants of 3CAmn varied with concentration and tail length; diffusion constants of DPPC and 3CAm19 increased with increasing 3CAm19 concentration at 300 K and shorter 3CAmn tails had higher diffusion constants at both temperatures. These computational studies provide a comprehensive understanding of the biophysical changes to model biological membranes by the association of 3CAmn.

INTRODUCTION

Biological cell membranes are a fluid mosaic comprising a phospholipid bilayer with multiple varieties of lipids and proteins. Studying phospholipid bilayers can give insight into the molecular interactions within the highly complex system that is the biological cell membrane. A wide variety of phospholipids can be found in cell membranes, such as 1,2-dipalmitoyl-*sn*-glycero-3-phosphatidylcholine (DPPC) shown in Figure 1, which is one of most commonly studied phospholipids in experimental and molecular simulation studies.[1−6] Introducing various molecules into a bilayer system can affect the biophysical properties (structure and dynamics) to such an extent that the biological functionality of the lipid bilayer is enhanced or hindered. Functional biological membranes are typically in the disordered, liquid-crystalline state as opposed to the ordered, gel state. Bilayers exhibit the liquid-crystalline state at temperatures above their main phase transition temperature, T_m, which for pure DPPC bilayers is well-known and characterized from both simulations and experimental measurements.[7,8] Recent simulation efforts have attempted to improve the precision of calculating T_m of DPPC.[9,10]

Dendritic amphiphiles, water-soluble molecules that contain very hydrophobic moieties, have demonstrated anti-HIV, anti-STD, antibacterial, antifungal, and antimycobacterial properties.[11−17] Why dendritic amphiphiles are so effective remains an unanswered question. Dendritic amphiphiles might cause changes in the phospholipid bilayer that is located in the cell envelope. These changes can result from either direct (e.g., binding to a target protein) or indirect (e.g., changing membrane thickness or fluidity) effects.

Received: October 10, 2012
Revised: December 18, 2012
Published: January 18, 2013

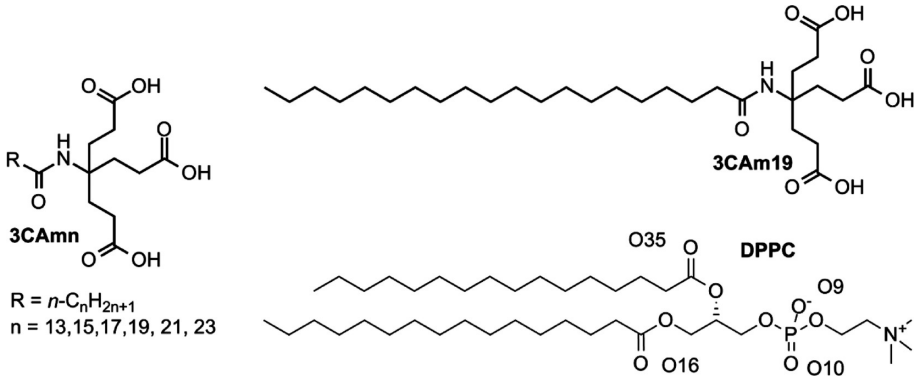

Figure 1. Chemical formulas of 3CAmn, 3CAm19, and DPPC.

Developing antimicrobials that selectively target microbial envelopes, rather than specific proteins, is our overarching goal. Antimicrobials that target either the organization of a microbial membrane or the functions of membrane-associated proteins have therapeutic potential against slow-growing or dormant microbial infections.[18] Introducing dendritic amphiphiles into membranes might cause nanometric environmental changes in fluidity and thickness; both can affect the operation of signaling, metabolism, and transport.[19] In this regard, dendritic amphiphiles might create lipid domains, serve as allosteric effectors of protein action, or distort bilateral lipid asymmetry; all could serve as primary or secondary mechanisms of action for killing microbes. Further, the mild detergent action of dendritic amphiphiles could result in the selective loss of specific membrane lipids.[20] As a consequence, changes in the membrane lipid composition, membrane fluidity, and membrane thickness can result in profound changes in the function of membrane-associated enzymes, transporters, regulatory proteins, and signaling proteins.

In order to gain insight into how dendritic amphiphiles interact with phospholipid bilayer membranes, we have undertaken molecular simulation studies. Dendritic amphiphiles are typically composed of three (or two) carboxylic acid head groups, which are connected to a hydrocarbon tail by an amido, carbamato, or ureido link. The general chemical formula for the class with three carboxylic acids with an amido link is $RCONHC(CH_2CH_2COOH)_3$, where R stands for hydrocarbon tail. The simplest class, which mimics natural fatty acids, has a single saturated alkyl chain (C_nH_{2n+1}). The shorthand notation for this class is 3CAmn; homologue with R = $C_{19}H_{39}$, 3CAm19, shown in Figure 1, has shown highly effective antimycobacterial properties.[17] As there are potentially significant roles of this molecule in pharmaceutical applications, one must understand the interactions of these molecules with the biological cell membrane, including fundamental studies with experimental measurements and molecular simulations.[21]

MD simulation is a computational approach to observe detailed molecular interactions and the changes resulting from those interactions. In this study, we report results from simulations aimed to observe and quantify the molecular interactions between dendritic amphiphiles, at different concentrations and of different tail lengths in a model cell membrane represented by a DPPC bilayer. We quantify the biophysical changes to the lipid bilayer in the presence of dendritic amphiphiles by analyzing the deuterium order parameter, bilayer thickness, lateral bilayer area, area per lipid and amphiphile, radial distribution function, and lateral diffusion constants. Qualitative changes in lipid tail tilt are also observed.

SIMULATION METHODS

MD simulations of DPPC bilayers with varying molar ratios of 3CAm19/DPPC were performed by using the molecular simulation package GROMACS (version 4.5.4).[22−24] In addition, DPPC bilayers with 3CAmn of various tail lengths, at a constant 3CAmn/DPPC ratio, were simulated. The bilayers were constructed by aligning the DPPC and 3CAmn molecules in a 12 × 12 grid with 3CAmn molecules randomly positioned. Each bilayer leaflet contained 144 molecules (3CAmn + DPPC). The bilayers were hydrated at a ratio of 40 water molecules per lipid for a total of 11,520 water molecules in each bilayer system. Five different molar ratios of 3CAm19/DPPC, 0.1, 0.2, 0.3, 0.4, and 0.5, and a pure DPPC bilayer control were simulated at both 300 and 325 K, to represent below and above the T_m of DPPC. Additional simulations were also performed for five different tail lengths of 3CAmn, for n = 13, 15, 17, 21, 23, at a 0.3 molar ratio at 300 and 325 K. A total of 22 different systems were simulated. Figure 2 provides a visual example of one such system. Table 1 shows the composition of bilayer leaflets at each molar ratio simulated.

The force field for DPPC and water were consistent with those employed in previous studies,[25−28] which was based in the parameters from Berger et al.[29] and partial atomic charges obtained from Chiu et al.[30] The single point charge (SPC)

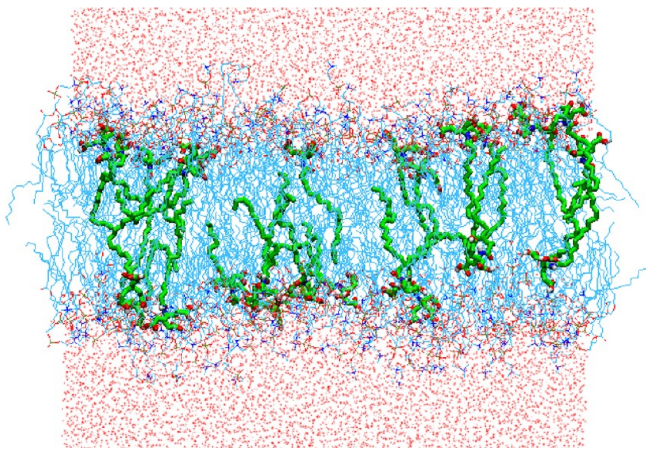

Figure 2. Snapshot of an equilibrated bilayer system with a 0.1 molar ratio of 3CAm19/DPPC at 325 K. Water molecules are shown in red, DPPC molecules in light blue, and 3CAm19 molecules in dark green.

dx.doi.org/10.1021/jp310043a | J. Phys. Chem. B 2013, 117, 1810−1818

Table 1. Compositions of Bilayers at Each 3CAm19 Concentration

molar ratio 3CAm19/DPPC	3CAm19 per leaflet	DPPC per leaflet
0	0	144
0.1	13	131
0.2	24	120
0.3	33	111
0.4	41	103
0.5	48	96

model was adopted for water.[31] For 3CAmn, the parameters for the headgroup were derived from fatty acids in the OPLS-UA force field,[32] while the hydrocarbon tail parameters were the same as those for DPPC. The united-atom representation was used for the methyl/methylene groups in the acyl chains of both DPPC and 3CAmn.

After initial construction of the systems, the bilayers were compressed and equilibrated to the desired simulation conditions. This was accomplished by initially performing simulations of the bilayer systems at higher pressure (up to 100 bar) and low temperature (200 K) for 0.5 ns. Next, to introduce disorder and achieve a local minimum energy, the bilayers were annealed to raise the temperature to 400 K at 1 bar, and then the temperature was decreased to either 300 or 325 K over a period of 2 ns. Once equilibrated, all systems were simulated in the constant pressure and constant temperature (NPT) ensemble at a temperature of 300 or 325 K and a pressure of 1 bar. Temperature was held constant using the V-Rescale algorithm and pressure was held constant using the Berendsen weak coupling method[33] with correlation times of τ_T = 0.1 ps and τ_P = 4.0 ps for temperature and pressure, respectively. Production simulations were run for at least 100 ns or until the system was fully equilibrated. Proper equilibration of each bilayer was recognized when the lateral area of the bilayer reached a steady value. For each bilayer system, the final 20 ns of simulation time were used in the analysis for the biophysical properties.

A time-step of 2 fs was used for all simulations. The linear constraint solver (LINCS) algorithm[34] was used to constrain all bonds of the lipid molecules, and the SETTLE algorithm[35] for water molecules. Coulombic and van der Waal cutoff interactions were at 1.0 nm. Long-range electrostatic interactions were corrected with the particle-mesh Ewald (PME) method[36,37] (0.12 nm for the grid size, fourth-order spline interpolation, and real-space cutoff at 1.0 nm). Periodic boundary conditions were applied in all directions. Trajectories were collected every 20 ps.

RESULTS AND DISCUSSION

Phospholipid bilayers exhibit two main phases: gel and liquid-crystalline. The gel phase, a more ordered phase, is characterized by straighter and more rigid lipid tails relative to the liquid-crystalline phase. The disordered liquid-crystalline phase sees a higher degree of bending and fluidity in the lipid tails. An order parameter, $-S_{cd}$, calculation quantifies the amount of order along the lipid tail, such that lower values for $-S_{cd}$ indicate more disorder and bending. Lipid tails in a gel, ordered state show order parameter curve similar to the one in Figure 3 for the pure DPPC bilayer at 300 K (solid black line). As shown, order increases in the upper region of the lipid tails for high 3CAm19 concentrations. For the DPPCs neighboring 3CAm19, the upper half of the chains contacts the more rigid portions (headgroup) of the amphiphile molecules, which reduces the conformational freedom. On the other hand, the lower half contacts the skinnier and more flexible 3CAm19 tails, which allows kinks in the DPPC tails. Also, as the single tail of 3CAm19 replaces the double tail of DPPC at higher 3CAm19 concentrations, fewer tails in the nonpolar region result in less packing. The 0.1 molar ratio at 300 K has an order parameter curve similar to the pure DPPC bilayer, suggesting that 3CAm19 at such a low concentration negligibly affects disorder of lipid tails. The order parameter curve for the 0.2 molar ratio has an apparent downward sloping trend, similar to lipid tails in disordered bilayers. Higher molar ratios of 3CAm19 (especially 0.4 and 0.5) induce a great decrease in conformational order at the tail ends of the DPPC, thus, producing an order profile with the general features observed for phospholipid bilayers in the liquid crystalline phase, while at temperatures below the phase transition temperature of pure DPPC bilayers. It is possible that a ratio of 0.2 3CAm19/DPPC is the lower limit for the system to undergo a transition from gel to liquid-crystalline, at 300 K.

Bilayers at 325 K already possess a high level of disorder in lipid tails. The data suggest that with increasing 3CAm19 in these liquid-crystalline bilayers, lipid tails are less disordered.

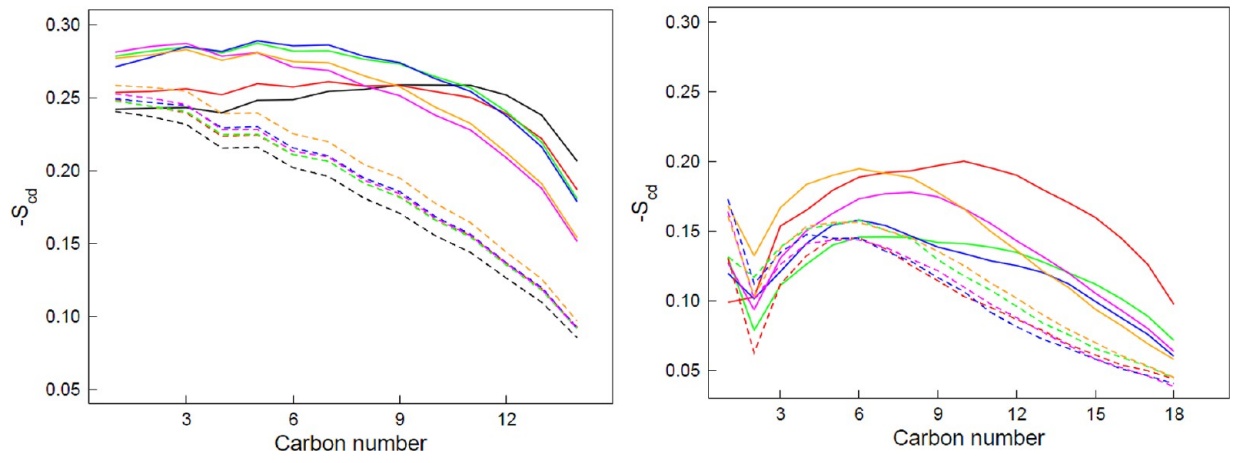

Figure 3. (left) Deuterium order parameter of DPPC hydrocarbon tails. The average curve between Sn-1 and Sn-2 tails are shown. (right) Deuterium order parameters of 3CAm19 hydrocarbon tails. Colors represent molar ratios of 3CAm19/DPPC such that black, pure DPPC bilayer; red, 0.1; green, 0.2; blue, 0.3; pink, 0.4; orange, 0.5. Solid lines represent systems at 300 K; dashed lines represent systems at 325 K.

dx.doi.org/10.1021/jp310043a | J. Phys. Chem. B 2013, 117, 1810−1818

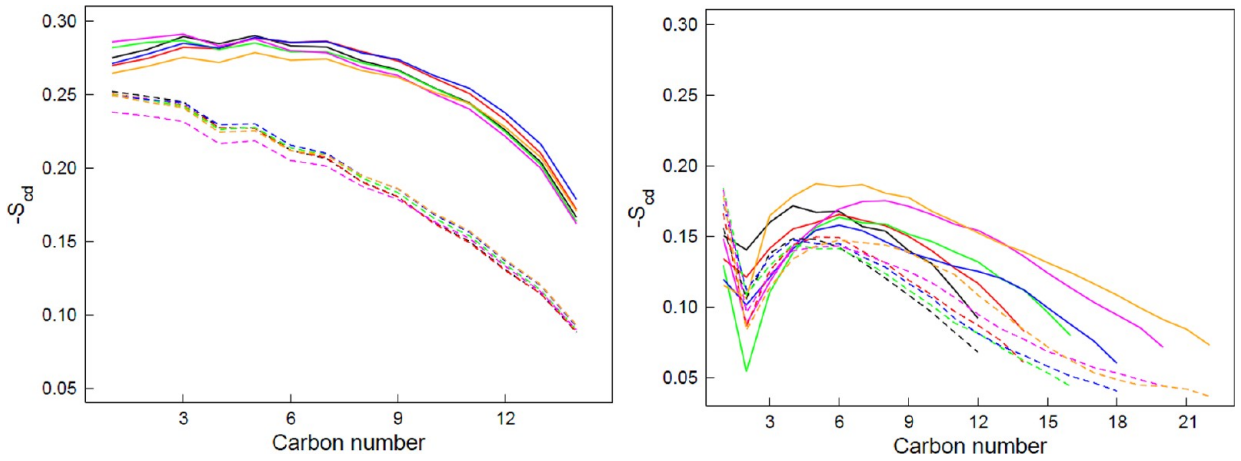

Figure 4. (left) Deuterium order parameter of DPPC in systems with varying 3CAmn tail length. (right) Deuterium order parameters of 3CAmn hydrocarbon tails. Colors represent number of carbons in 3CAmn tails such that black, C_{13}; red, C_{15}; green, C_{17}; blue, C_{19}; pink, C_{21}; orange, C_{23}. Solid lines represent systems at 300 K; dashed lines represent systems at 325 K.

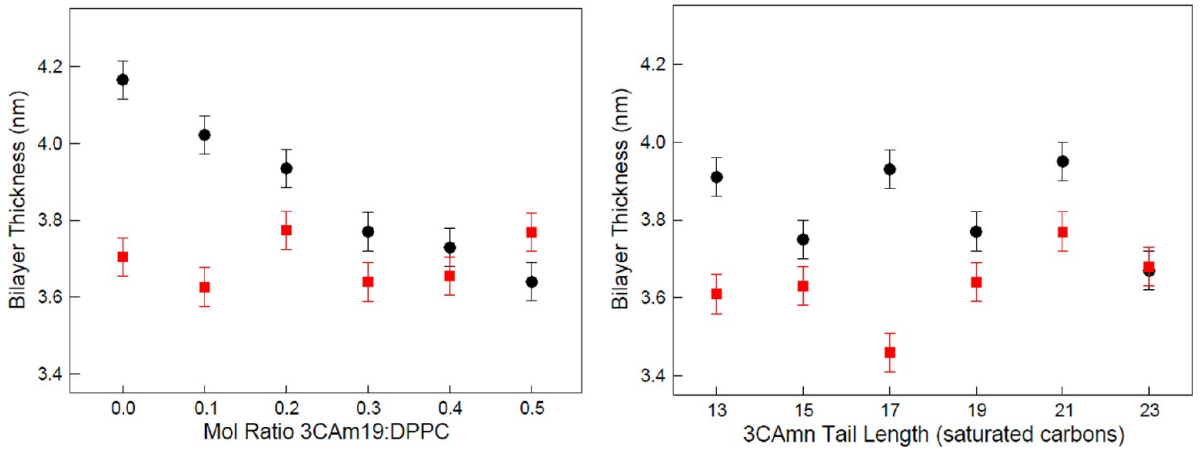

Figure 5. Bilayer thickness calculated as the average distance between phosphate groups of DPPC for simulations varying 3CAm19 concentration (left) and 3CAmn tail length (right) in DPPC bilayers. Black circles and red squares represent systems at 300 and 325 K, respectively. Error bars are estimated from the deviation in the measured thickness over time.

This may be caused by an increase in hydrogen bonding with higher concentrations of 3CAm19 in the bilayer. Hydrogen bonding ties molecules together and prevents mobility. Figure 3 also shows the order parameters for the tail of 3CAm19. Reinforced in these data is the evidence that the 0.1 molar concentration exhibits the most ordered bilayer and that increasing 3CAmn concentration decreases the order at 300 K. The DPPC order parameters for simulations with varying 3CAmn tail lengths, shown in Figure 4, resemble the 0.3 concentration of 3CAm19 order parameter curves. This suggests that tail length of 3CAmn does not have a significant effect on the disorder of DPPC tails in the bilayer. Longer 3CAmn tails, however, exhibit higher levels of order at 300 K, perhaps due to increased atomic density in the nonpolar region of the bilayer.

The bilayer thickness, defined as the average distance between the phosphate groups of DPPC of opposite leaflets, was calculated and results are shown in Figure 5. Increasing concentrations of 3CAm19 results in decreasing bilayer thickness at 300 K. Bilayer thickness data in conjunction with order parameter trends for varying concentrations of 3CAm19, suggest increasing concentrations of 3CAm19 in DPPC bilayers at 300 K cause more disorder and kinks in the lipid tails, leading to increased tail bending and interdigitation of tail ends from opposite leaflets. The 0.2 3CAm19/DPPC bilayer achieves a bilayer thickness near that of a pure DPPC bilayer at its phase transition temperature (~3.9 nm at 315 K[7,38]). Molar ratios above 0.4 and 0.5 show no change in bilayer thickness between 300 and 325 K. It can be deduced that higher 3CAm19 concentrations in a DPPC bilayer causes the phase transition temperature of the system to decrease, expanding the temperature range for the liquid-crystalline phase to include 300 K, a temperature that would encourage the gel phase for pure DPPC. At 325 K, however, the bilayer thickness remains relatively unchanged across all concentrations of 3CAm19. This is because the slight increase in ordering with increasing 3CAm19 concentration (seen in the order parameter of bilayers at 325 K) in an overall disordered system is not enough to straighten lipid tails.

Bilayer thickness data are harder to interpret for the variation in tail lengths. For all tail lengths except the longest, C23, a significant difference occurs between the thicknesses of the bilayers at the two temperatures simulated. For bilayers with C23, however, there is no change in the bilayer thickness with a 25 K temperature change from below the DPPC phase transition temperature to above it. Snapshots of these bilayers

dx.doi.org/10.1021/jp310043a | J. Phys. Chem. B 2013, 117, 1810−1818

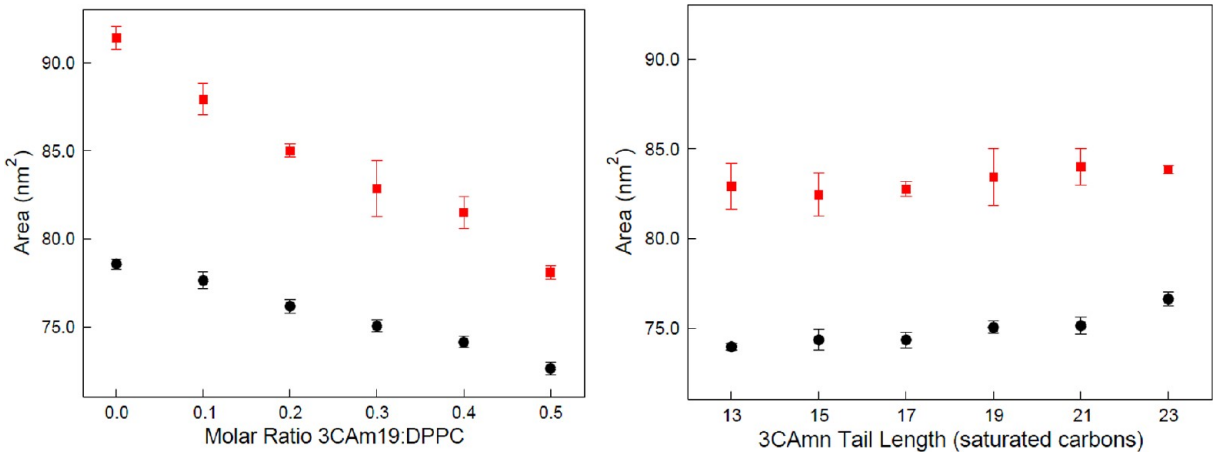

Figure 6. Lateral bilayer area averaged over a 20 ns period in which the systems are equilibrated. Black circles and red squares represent systems at 300 and 325 K, respectively. Error bars are estimated from the deviation in the measured area over time.

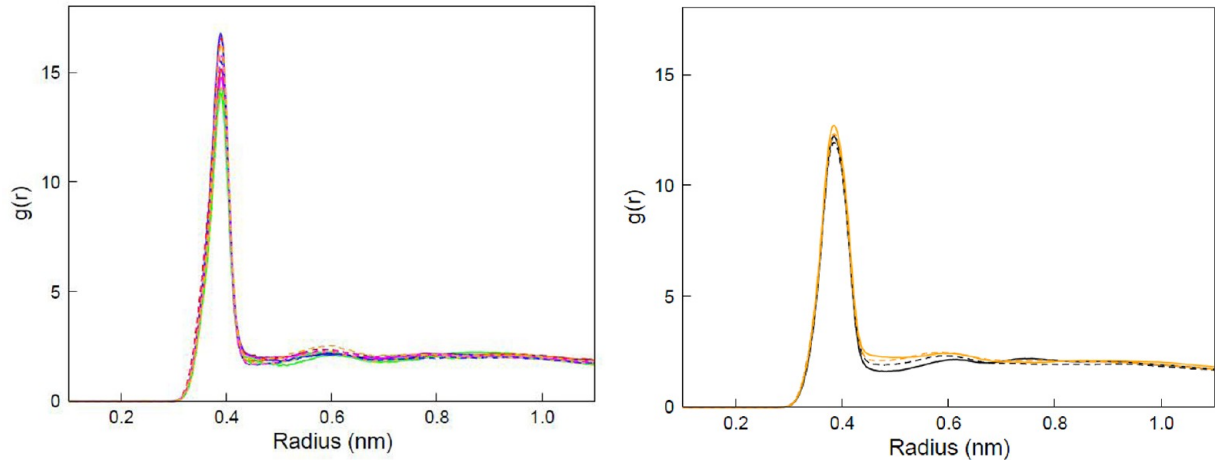

Figure 7. Radial distribution function curves of carboxylic heads of 3CAmn (hydrogen donors) to phosphate group of DPPC (hydrogen acceptor). Left shows overlaid curves of all 12 varying concentration simulations. Right shows overlaid curves for 4 of the 12 varying tail length simulations. Solid lines represent systems at 300 K; dashed lines represent systems at 325 K. Color descriptions are explained in Figures 3 and 4, respectively.

show that the 3CAm23 tails bend significantly and do not interdigitate at both lower and higher temperatures, while shorter tails remain straight at lower temperatures. The bending of the 3CAm23 tail induces disorder and hinders the gel state in the DPPC tails because it prevents tight packing of straight DPPC tails.

Uniform tilt angle in lipid tails is another metric used to identify gel phase bilayers. For simulations at 300 K, snapshots of the *xz* plane of the bilayer qualitatively show a gradual change in the tilt angle of lipid tails with increasing 3CAm19 concentration, shown in Figure S1 of the Supporting Information. At molar ratios 0.4 and above, tilt angle is visibly zero, indicative of liquid-crystalline behavior. The combined results of the deuterium order parameter, bilayer thickness and qualitative observations of lipid tail tilt show that a molar ratio of 0.2 3CAm19/DPPC marks the lower limit of 3CAm19 concentration to induce a phase transition from gel to liquid-crystalline at 300 K, while the 0.4 molar ratio is completely liquid-crystalline at 300 K.

Bilayers at 325 K are seen to have a larger lateral bilayer area relative to bilayers at 300 K, shown in Figure 6, due to increased tail bending, which causes lipid molecules to push away from each other rather than pack together neatly. In addition, a significant trend is seen in bilayers at both temperatures for the lateral bilayer area with varying 3CAm19 concentrations. The lateral area decreases with increasing 3CAm19 concentrations. The radial distribution function and the chemical structure of the 3CAmn molecule provide insight to explain this phenomenon. The radial distribution function (RDF) provides information on the probability of a moiety at a certain radius away from another moiety. A peak in the RDF curve around 0.4 nm indicates hydrogen bonding between the two moieties. RDF curves were found for two different potential hydrogen bonding configurations. The first arrangement analyzed was the three carboxylic acids of 3CAmn (hydrogen-bond donors) in relation to the phosphate group on DPPC (hydrogen-bond acceptor), shown in Figure 7. The peak occurring at a radius of 0.4 nm indicates hydrogen bonding between the two groups. All systems show similar peaks, indicating that regardless of concentration, 3CAmn tail length, or temperature, there is hydrogen bonding occurring between DPPC and 3CAmn head groups within the bilayer system. The second arrangement analyzed was the amide on 3CAmn (hydrogen-bond donor) with one of four different oxygen atoms on DPPC (hydrogen-bond acceptors). Consistent throughout all five systems of varying 3CAmn concentration

dx.doi.org/10.1021/jp310043a | *J. Phys. Chem. B* 2013, 117, 1810−1818

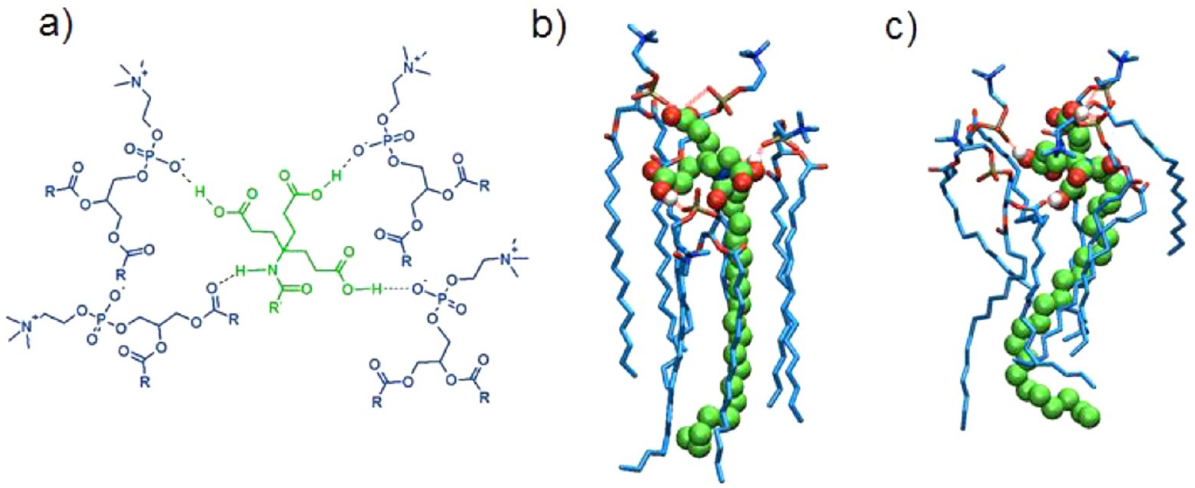

Figure 8. (a) Hydrogen bonding pattern between a single 3CAmn molecule (green) and four DPPC molecules (blue) at the carboxylic acids and amide. (b) 3-D representation of the hydrogen bonding and tail order of 3CAm19 at 300 K and (c) 3CAm23 at 325 K.

at both 300 and 325 K was a peak for the amide-O35 curve, indicative of hydrogen bonding between the amide of 3CAmn and the carbonyl group for the sn-2 tail of DPPC shown in Figure S2 of Supporting Information. Also observed were peaks that indicate hydrogen bonding between amide-O16, the carbonyl group of the sn-1 tail of DPPC. The two oxygen atoms in the phosphate group of the DPPC did not show hydrogen-bonding peaks. The same result is seen in the relationships between the carbonyl oxygens on DPPC and the amide of 3CAmn for the systems with varying 3CAmn tail length in Figure S3 of Supporting Information. Figure 8 shows the overall hydrogen bonding pattern between a central 3CAm19 and four DPPC molecules and a visualization of the three-dimensional conformation of the molecules in the ordered and disordered phases (the snapshots are adjusted to highlight the bonding pattern eliminating any tilt angle relative to the *z*-axis). Higher concentrations of 3CAm19 in the bilayer offer more hydrogen bonding opportunities between the three carboxylic acids and one amide on 3CAm19 to the phosphate and two carbonyl groups on the DPPC molecule. Because hydrogen bond lengths are smaller than all other intermolecular associations, increasing the number of hydrogen bonds causes a decrease the lateral area because molecules are more closely bound to each other.

Structurally, the headgroup of the 3CAm19, which consists of three carboxylic acids, is much smaller than the headgroup of DPPC, which includes a phosphate group and a choline moiety. To quantify this, two methods were used and compared to obtain the area per headgroup for each molecule in the bilayer leaflets. The first method was proposed by Leekumjorn et al.[39] who suggested a linear relationship between the area per DPPC and concentration of 3CAmn in a bilayer. This method also suggested that the areas per DPPC and 3CAmn are independent of concentration. The line fit method for bilayers at 300 K, shown in Figure 9, reveals in an area per DPPC headgroup of 0.55 nm^2 and an area per 3CAmn headgroup of 0.09 nm^2. To compare these values, a second method obtained the area per DPPC and 3CAmn headgroup by a Voronoi tessellation of the lateral surface of each leaflet. The center of mass coordinates of the headgroup of each molecule (choline and phosphate groups on DPPC and all three carboxylic acids on 3CAmn) were used to represent each molecule as a single

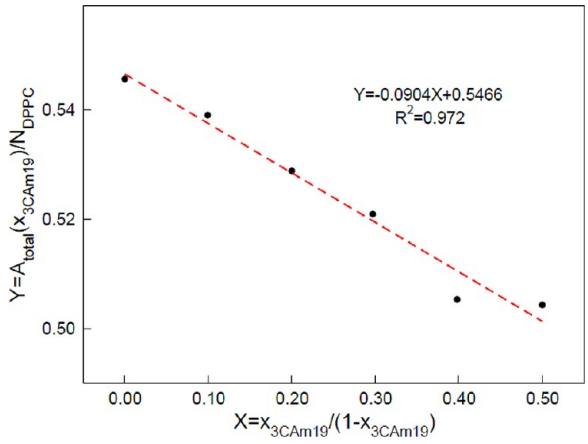

Figure 9. Line-Fit method to determine the area per DPPC and 3CAmn with systems at 300 K. The slope of the fit line is the area per 3CAmn, and the *y*-intercept is the area per DPPC, in nm^2, displayed in inset equation.

point. The Voronoi tessellation drew lines equidistantly between each point to create polygons around each point that represented the area of the molecules headgroup. Diagrams of Voronoi tessellations of two leaflets are shown in Figure S4 of the Supporting Information. Areas were calculated and averaged from over 100 coordinate files, each containing two leaflets, from the equilibrated bilayers trajectory. To account for the periodic boundary conditions of the simulation, and to eliminate and unclosed Voronoi polygons, the tessellation of the bilayer includes translations of the original leaflet on all four sides. The areas per lipid and 3CAmn values are of the original 144 atoms in the leaflet. The areas per DPPC and 3CAmn headgroup obtained by this Voronoi method are shown in Figure 10.

The Voronoi method is likely to give more precise answers, because it is not an approximation, but rather an average of thousands of sample area per lipid and area per 3CAmn data points over the 20 ns period of equilibration in the bilayers. At 300 K, the Voronoi method sees an area per DPPC of around 0.55 nm^2, which closely resembles that derived by the line fit method. However, the area per 3CAmn headgroup was found to be around 0.45 nm^2. 3CAmn takes up less space in the polar

dx.doi.org/10.1021/jp310043a | J. Phys. Chem. B 2013, 117, 1810−1818

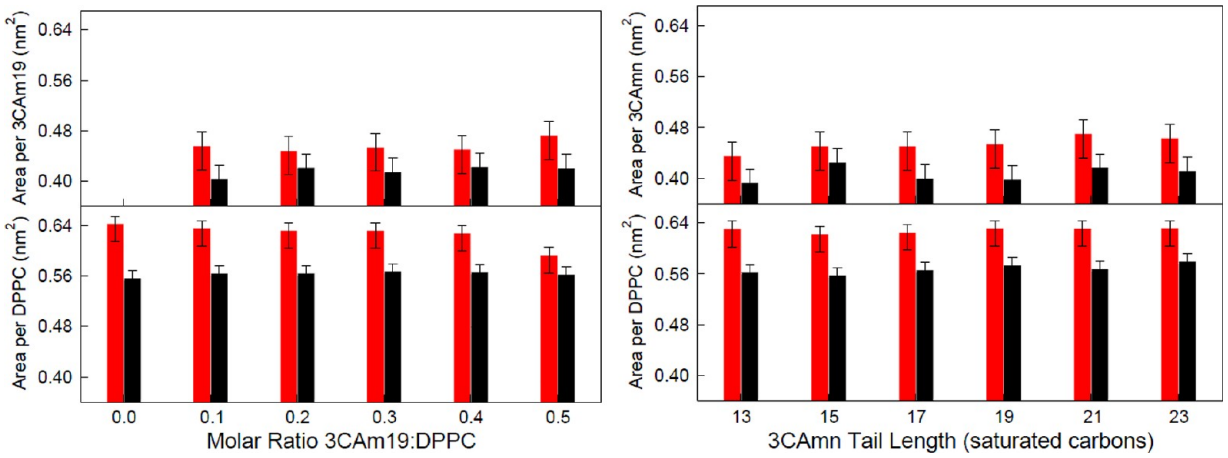

Figure 10. Areas per DPPC and 3CAmn obtained using the Voronoi method with respect to 3CAmn concentration (left) and 3CAmn tail length (right). Black bars represent systems at 300 K; red symbols represent systems at 325 K.

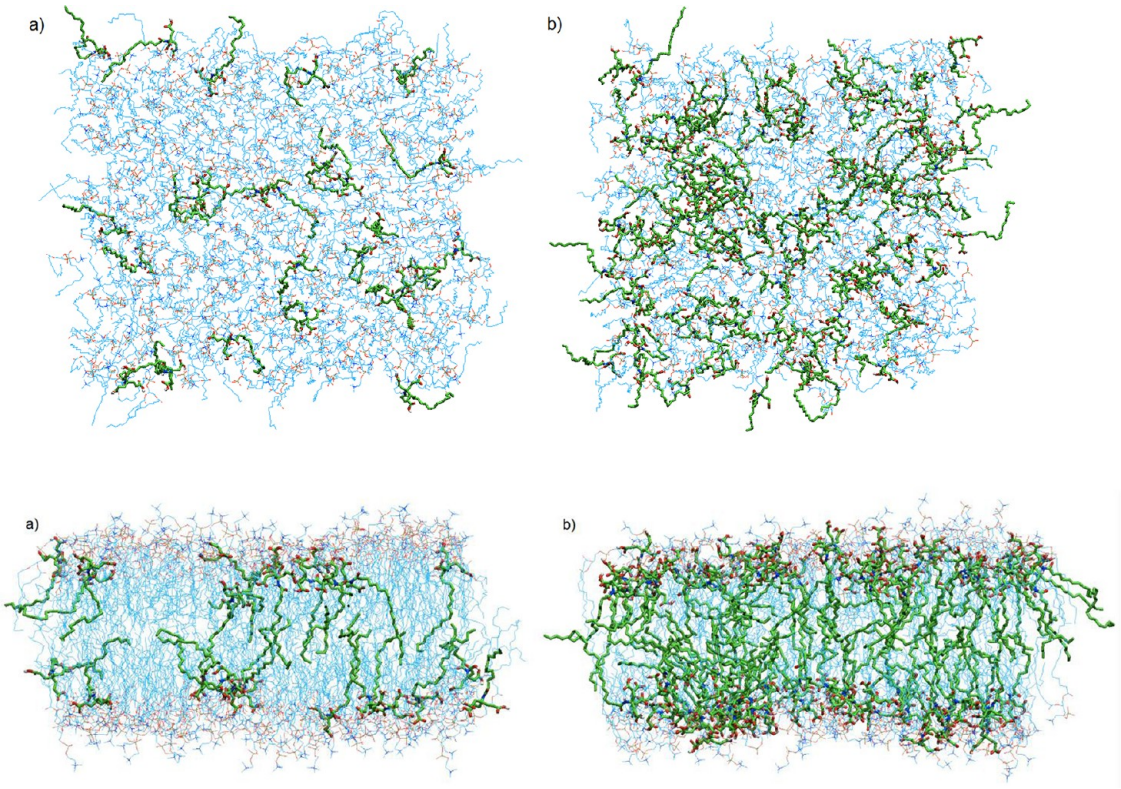

Figure 11. (top) Side views of bilayer systems at 325 K and (a) 0.1 molar ratio and (b) 0.5 molar ratio. (bottom) Top views of bilayer systems at 325 K and (a) 0.1 molar ratio and (b) 0.5 molar ratio. Water is removed for clarity. DPPC is depicted as light blue thin lines; 3CAm19 is depicted as dark green thick lines.

region of the bilayer, and therefore with a higher concentration of 3CAm19 in the bilayer, the lateral area shrinks because of the higher proportion of smaller 3CAm19 head groups. At 300 K, lateral area increases in the bilayer with longer 3CAmn tails. In this case, an increased bilayer surface area corresponds to decreased acyl chain ordering and increased membrane fluidity, shown in the order parameter data from Figure 6. Figure 11 visually represents the changes in bilayer thickness and lateral bilayer area at 325 K.

The mean-squared displacement (MSD) is a measure that provides information on the average lateral, two-dimensional diffusion of DPPC and 3CAmn molecules in the plane of the bilayer over the simulation. The lateral diffusion constant, D, can be determined from the mean squared displacement by

$$D = \lim_{t\to\infty}\left(\frac{[r(t) - r(0)]^2}{2dt}\right)$$

where $r(t)$ is the position at time t, $[r(t) - r(0)]^2$ is the MSD, and d is the number of dimensions in which diffusion is occurring ($d = 2$ in the bilayer). This equation can be linearized and the results line with unity slope has a y-intercept that can be used to calculate the diffusion constant. An example mean-squared displacement curve fit for DPPC and 3CAm19 in a bilayer at 0.2 molar ratio and 300 K is shown in the Figure S5

dx.doi.org/10.1021/jp310043a | J. Phys. Chem. B 2013, 117, 1810−1818

of Supporting Information. When a line of slope = 1 is fit to the end region of the curves, 10 is raised to the *y*-intercept of the line, and the value divided by 2*d* to obtain the diffusion constant, *D*. DPPC and 3CAmn diffusion constants for all 22 simulations are shown in Tables 2 and 3. The calculated values

Table 2. Diffusion Constants for DPPC and 3CAmn in Varying Molar Ratio Systems

temperature (K)	3CAm19 molar ratio	D_{DPPC}[a]	D_{3CAm19}[a]
300	0.0	0.04 ± 0.01	
	0.1	0.06 ± 0.01	0.07 ± 0.01
	0.2	0.09 ± 0.01	0.10 ± 0.01
	0.3	0.13 ± 0.01	0.16 ± 0.01
	0.4	0.14 ± 0.01	0.17 ± 0.01
	0.5	0.22 ± 0.01	0.22 ± 0.01
325	0.0	0.19 ± 0.01	
	0.1	0.19 ± 0.01	0.18 ± 0.01
	0.2	0.20 ± 0.01	0.20 ± 0.01
	0.3	0.18 ± 0.01	0.18 ± 0.01
	0.4	0.18 ± 0.01	0.17 ± 0.01
	0.5	0.22 ± 0.01	0.25 ± 0.01

[a]Values reported as $D \times 10^6$ cm^2/s.

Table 3. Diffusion Constants for DPPC and 3CAmn in All Varying Tail Length Systems[a]

temperature (K)	3CAmn tail length	D_{DPPC}[b]	D_{3CAmn}[b]
300	*n* = 13	0.06 ± 0.01	2.50 ± 0.01
	n = 15	0.14 ± 0.01	1.77 ± 0.01
	n = 17	0.22 ± 0.01	1.00 ± 0.01
	n = 19	0.13 ± 0.01	0.16 ± 0.01
	n = 21	0.07 ± 0.01	0.08 ± 0.01
	n = 23	0.06 ± 0.01	0.06 ± 0.01
325	*n* = 13	0.40 ± 0.01	3.96 ± 0.01
	n = 15	0.14 ± 0.01	2.50 ± 0.01
	n = 17	0.25 ± 0.01	1.47 ± 0.01
	n = 19	0.13 ± 0.01	0.18 ± 0.01
	n = 21	0.25 ± 0.01	0.28 ± 0.01
	n = 23	0.14 ± 0.01	0.16 ± 0.01

[a]All systems for molar ratio of 0.3 3CAmn/DPPC. [b]Values reported as $D \times 10^6$ cm^2/s.

of D_{DPPC} for our simulations at 325 K is in line with the reported value for long-time D_{DPPC} in a pure DPPC bilayer at 323 K (0.12×10^{-6} cm^2/s).[40] Our simulation value of D_{DPPC} in a pure DPPC bilayer at 300 K is in the same order of magnitude as the upper limit of the range for experimental D_{DPPC} around 300 K ($0.04–16 \times 10^{-9}$ cm^2/s).[41] Deviations may be a result of the short time scale, around 100 ns, over which the diffusion constant is calculated. At 300 K, as more 3CAmn is introduced into an ordered DPPC bilayer system, disorder is created and higher degrees of lateral motion for 3CAmn and DPPC result, quantitatively shown in higher D_{DPPC} and D_{3CAm19} in Table 3. At 300 and 325 K, the tail length greatly affects the diffusion constant for 3CAmn. Shorter molecules have smaller surface area, which decreases drag effects. Longer 3CAmn tails get trapped and have lower lateral mobility within the bilayer.

CONCLUSIONS

The hydrophilic tricarboxylic headgroup and the hydrophobic tail facilitate the integration of the antimicrobial dendritic amphiphile 3CAmn into phospholipid bilayers, the foundational structure of biological cellular membranes. When 3CAmn dendritic amphiphilic molecules are mixed with DPPC in a bilayer, the molecular dynamics of the system change significantly. Data on the deuterium order parameter, bilayer thickness, and tail tilt angle shows increased disorder and tail kinking by the addition of 3CAmn. A molar ratio of 0.2 3CAm19/DPPC is believed to be sufficient to induce a phase transition from gel to liquid crystalline at 300 K. Higher concentrations of 3CAm19, especially 0.4 and 0.5 molar ratios, show strong evidence of liquid-crystalline behavior at 300 K. Increased 3CAm19 concentration decreases the phase transition temperature of the bilayer; as a result, the liquid-crystalline phase, which is required for biological cell membrane functionality, persists for a wider range of temperatures. Decreases in lateral bilayer area with the addition of 3CAmn can be explained in terms of increased hydrogen bonding (as evidenced by peaks in the RDF) and relative sizes of DPPC and 3CAmn head groups, with the exception of bilayers with 3CAm23. Larger lateral bilayer area for 3CAm23, relative to shorter tail lengths, is explained by the significant tail bending regardless of temperature, which hinders tight packing of molecules. Diffusion constants for DPPC and 3CAm19 at 300 K are increased by the increased 3CAm19 concentration; longer 3CAmn tails have lower diffusion constants due to increased drag. These data show evidence of prominent trends that exist for many biophysical properties of DPPC bilayers with the addition of 3CAmn in varying concentration or of varying tail length. Understanding the mechanism of biophysical changes to DPPC membranes by the addition of 3CAmn can provide initial thoughts on how dendritic amphiphile molecules can help or harm mammalian cells and possibly pave the way to a new line of pharmaceuticals. Further investigation could lead to the quantification of the phase transition temperature change associated with added 3CAmn in DPPC bilayers. Also, further insights into the mechanism of action of dendritic amphiphiles in cellular membranes could entail exploring how these molecules affect more complex phospholipid bilayer models that include a variety of lipids and even proteins.

ASSOCIATED CONTENT

Supporting Information

Side views of bilayers at 300 K qualitatively displaying decrease of lipid tail tilt with increasing 3CAm19 concentration (Figure S1); RDF curves for the interactions between the amide of 3CAm19, and four different oxygen sites of DPPC for all 22 simulations (Figures S2 and S3); diagrams of Voronoi tessellations of two leaflets (Figure S4); and mean-squared displacement curve fit for DPPC and 3CAm19 in a bilayer at 0.2 molar ratio and 300 K (Figure S5). This material is available free of charge via the Internet at http://pubs.acs.org.

AUTHOR INFORMATION

Corresponding Author

*Tel.: +1 (303) 273-3873. Fax: +1 (303) 273-3730. E-mail: asum@mines.edu.

Notes

The authors declare no competing financial interest.

■ ACKNOWLEDGMENTS

This project was partially funded from the DuPont Young Professor Award to A.K.S. All the simulations were performed with computational resources in Ra at the Colorado School of Mines, which is part of the GECO (Golden Energy Computing Organization).

■ REFERENCES

(1) De Vries, A.; Marrink, S.; Mark, A. In 47th Annual Meeting of the Biophysical Society, March 1−5, 2003, San Antonia, TX, Biophysical Society: Rockville, MD, 2003; Vol. *84*.
(2) Egberts, E.; Marrink, S. J.; Berendsen, H. J. *Eur. Biophys. J.* **1994**, *22*, 423−36.
(3) Feller, S. E.; Venable, R. M.; Pastor, R. W. *Langmuir* **1997**, *13*, 6555−6561.
(4) Tieleman, D. P.; Berendsen, H. J. C. *J. Chem. Phys.* **1996**, *105*, 4871.
(5) Sega, M.; Garberoglio, G.; Brocca, P.; Cantù, L. *J. Phys. Chem. B* **2007**, *111*, 2484−9.
(6) Sega, M.; Vallauri, R.; Brocca, P.; Cantù, L.; Melchionna, S. *J. Phys. Chem. B* **2007**, *111*, 10965−9.
(7) Leekumjorn, S.; Sum, A. K. *Biochim. Biophys. Acta* **2007**, *1768*, 354−65.
(8) Petrov, A. G.; Gawrisch, K.; Brezesinski, G.; Klose, G.; Möps, A. *Biochim. Biophys. Acta, Biomembr.* **1982**, *690*, 1−7.
(9) Schubert, T.; Schneck, E.; Tanaka, M. *J. Chem. Phys.* **2011**, *135*, 055105.
(10) Coppock, P. S.; Kindt, J. T. *J. Phys. Chem. B* **2010**, *114*, 11468−73.
(11) Sugandhi, E. W.; Falkinham, J. O.; Gandour, R. D. *Bioorg. Med. Chem.* **2007**, *15*, 3842−53.
(12) Sugandhi, E. W.; Macri, R. V; Williams, A. A; Kite, B. L.; Slebodnick, C.; Falkinham, J. O.; Esker, A. R.; Gandour, R. D. *J. Med. Chem.* **2007**, *50*, 1645−50.
(13) Sugandhi, E. W.; Slebodnick, C.; Falkinham, J. O.; Gandour, R. D. *Steroids* **2007**, *72*, 615−26.
(14) Williams, A. a; Sugandhi, E. W.; Macri, R. V; Falkinham, J. O.; Gandour, R. D. *J. Antimicrob. Chemother.* **2007**, *59*, 451−8.
(15) Macri, R. V; Karlovská, J.; Doncel, G. F.; Du, X.; Maisuria, B. B.; Williams, A. a; Sugandhi, E. W.; Falkinham, J. O.; Esker, A. R.; Gandour, R. D. *Bioorg. Med. Chem.* **2009**, *17*, 3162−8.
(16) Maisuria, B. B.; Actis, M. L.; Hardrict, S. N.; Falkinham, J. O.; Cole, M. F.; Cihlar, R. L.; Peters, S. M.; Macri, R. V; Sugandhi, E. W.; Williams, A. A.; Poppe, M. A.; Esker, A. R.; Gandour, R. D. *Bioorg. Med. Chem.* **2011**, *19*, 2918−2926.
(17) Falkinham, J. O.; Macri, R. V; Maisuria, B. B.; Actis, M. L.; Sugandhi, E. W.; Williams, A. A.; Snyder, A. V; Jackson, F. R.; Poppe, M. A.; Chen, L.; Ganesh, K.; Gandour, R. D. *Tuberculosis* **2012**, *92*, 173−81.
(18) Hurdle, J. G.; O'Neill, A. J.; Chopra, I.; Lee, R. E. *Nat. Rev.* **2011**, *9*, 62−75.
(19) Van Meer, G.; Voelker, D. R.; Feigenson, G. W. *Nat. Rev. Mol. Cell Biol.* **2008**, *9*, 112−24.
(20) Quinn, P. J. In *Lipids and Essential Oils as Antimicrobial Agents*; John Wiley & Sons, Ltd.: New York, 2011; pp 1−24.
(21) Karlovská, J.; Williams, A. a; Macri, R. V; Gandour, R. D.; Funari, S. S.; Uhríková, D.; Balgavý, P. *Colloids Surf., B* **2007**, *54*, 160−4.
(22) Berendsen, H. J. C.; Van der Spoel, D.; Van Drunen, R. *Comput. Phys. Commun.* **1995**, *91*, 43−56.
(23) Hess, B.; Uppsala, S.-; Lindahl, E. *J. Chem. Theory Comput.* **2008**, 435−447.
(24) Van Der Spoel, D.; Lindahl, E.; Hess, B.; Groenhof, G.; Mark, A. E.; Berendsen, H. J. C. *J. Comput. Chem.* **2005**, *26*, 1701−18.
(25) Marrink, S.; Berger, O.; Tieleman, P.; Jahnig, F. *Biophys. J.* **1998**, *74*, 931−943.
(26) Leekumjorn, S.; Sum, A. K. *Biophys. J.* **2006**, *90*, 3951−65.
(27) Doxastakis, M.; Sum, A. K.; De Pablo, J. J. *J. Phys. Chem. B* **2005**, *109*, 24173−81.
(28) Leekumjorn, S.; Sum, A. K. *J. Phys. Chem. B* **2008**, *112*, 10732−40.
(29) Berger, O.; Edholm, O.; Jähnig, F. *Biophys. J.* **1997**, *72*, 2002−13.
(30) Chiu, S. W.; Clark, M.; Balaji, V.; Subramaniam, S.; Scott, H. L.; Jakobsson, E. *Biophys. J.* **1995**, *69*, 1230−45.
(31) Berendsen, H. J. C.; Postma, J. P. M.; Van Gunsteren, W. F.; Hermans, J. *Intermol. Forces* **1981**, 331−338.
(32) Jorgensen, W. L.; Maxwell, D. S.; Tirado-rives, J. *J. Am. Chem. Soc.* **1996**, *7863*, 11225−11236.
(33) Berendsen, H. J. C.; Postma, J. P. M.; Van Gunsteren, W. F.; DiNola, A.; Haak, J. R. *J. Chem. Phys.* **1984**, *81*, 3684.
(34) Hess, B.; Bekker, H.; Berendsen, H. J. C.; Fraaije, J. G. E. M. *J. Comput. Chem.* **1997**, *18*, 1463−1472.
(35) Miyamoto, S.; Kollman, P. A. *J. Comput. Chem.* **1992**, *13*, 952−962.
(36) Darden, T.; York, D.; Pedersen, L. *J. Chem. Phys.* **1993**, *98*, 10089.
(37) Essmann, U.; Perera, L.; Berkowitz, M. L.; Darden, T.; Lee, H.; Pedersen, L. G. *J. Chem. Phys.* **1995**, *103*, 8577.
(38) Rappolt, M.; Rapp, G. *Eur. Biophys. J.* **1996**, *24*, 381−386.
(39) Leekumjorn, S.; Wu, Y.; Sum, A. K.; Chan, C. *Biophys. J.* **2008**, *94*, 2869−83.
(40) Lindahl, E.; Edholm, O. *J. Chem. Phys.* **2001**, *115*, 4938.
(41) Lee, B.-S.; Mabry, S. A.; Jonas, A.; Jonas, J. *Chem. Phys. Lipids* **1995**, *78*, 103−117.